

Adaptive Adversarial Training to Improve Adversarial Robustness of DNNs for Medical Image Segmentation and Detection

Linhai Ma and Liang Liang

University of Miami, Coral Gables FL 33146, USA

`l.ma@miami.edu`

`liang@cs.miami.edu`

Abstract. Recent methods based on Deep Neural Networks (DNNs) have reached high accuracy for medical image analysis, including the three basic tasks: segmentation, landmark detection, and object detection. It is known that DNNs are vulnerable to adversarial attacks, and the adversarial robustness of DNNs could be improved by adding adversarial noises to training data (i.e., adversarial training). In this study, we show that the standard adversarial training (SAT) method has a severe issue that limits its practical use: it generates a fixed level of noises for DNN training, and it is difficult for the user to choose an appropriate noise level, because a high noise level may lead to a large reduction in model performance, and a low noise level may have little effect. To resolve this issue, we have designed a novel adaptive-margin adversarial training (AMAT) method that generates adaptive adversarial noises for DNN training, which are dynamically tailored for each individual training sample. We have applied our AMAT method to state-of-the-art DNNs for the three basic tasks, using five publicly available datasets. The experimental results demonstrate that our AMAT method outperforms the SAT method in adversarial robustness on noisy data and prediction accuracy on clean data. Please contact the author for the source code.

Keywords: Adversarial Robustness · Medical Image Segmentation · Landmark Detection · Object Detection.

1 Introduction

Recent methods based on Deep Neural Networks (DNNs) have achieved high accuracy for medical image analysis, including three basic tasks: segmentation, landmark detection, and object detection. However, DNNs are vulnerable to imperceptible adversarial noises [25, 3, 2, 6, 13, 18, 20, 17, 21] (Fig. 1), which makes it dangerous to deploy DNN-based decision-making systems for life-critical applications, such as medical image-based diagnosis. To make DNNs robust to adversarial noises, a tremendous amount of work has been done for natural images [9, 17, 3, 8, 16, 19, 22, 1, 4, 29, 32, 31]. As a comparison, in the field of medical image analysis, especially for the three basic tasks, the number of

defense methods [15, 10, 7] pales. Some of these defense methods are either not effective enough [27, 15] or only work for very limited network structures [10].

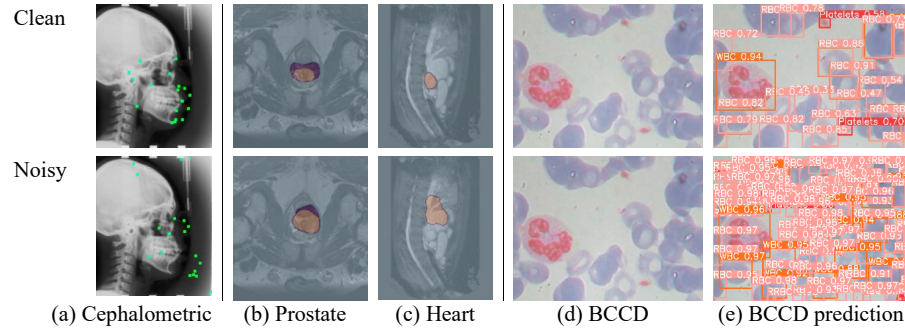


Fig. 1: Examples of adversarial attacks against cephalometric landmark detection (a), segmentation of prostate (b) and heart (c), and blood cell detection ((d) is the input image and (e) is the detection result). By adding adversarial noises to the original/clean images (the first row), the noisy images are obtained (the second row). DNN outputs are significantly changed when the input images contain adversarial noises.

To improve adversarial robustness of DNNs for classification-related tasks, the standard adversarial training (SAT) method [9, 14, 17] is often considered [7]: given a fixed noise level ε (Lp vector norm), generate a noisy/adversarial sample (\tilde{x}, y) using the PGD algorithm [17], where $\tilde{x} = PGD(x, y, \varepsilon)$ and $\|x - \tilde{x}\|_p \leq \varepsilon$, for every sample (x, y) in the training set; use the clean data $\{(x, y)\}$ and noisy data $\{(\tilde{x}, y)\}$ together to train the model. The SAT loss function is given in [9]:

$$L_{SAT} = (L(f(x), y) + L(f(\tilde{x}), y))/2 \quad (1)$$

where L is the original loss function for training the DNN model f . However, as will be shown in this study, the SAT method is problematic.

In our work to improve the adversarial robustness of DNNs for the three basic tasks (image segmentation, landmark detection, and object detection), we have made the following contributions. (1) We investigate the problem of SAT: when the training noise level ε increases, the performance of SAT-trained models improves on data with larger noises, but drops on clean data or data with smaller noises, which indicates that a fixed level of noise for training is inadequate. (2) To solve this problem, we design and implement a novel adaptive-margin adversarial training (AMAT) method that generates adaptive noises for training DNNs instead of using a fixed noise level. In this way, the trained DNN model has good resistance to adversarial noises while maintaining good accuracy on clean data. We apply our AMAT method to state-of-the-art DNNs on five publicly available datasets, and the results demonstrate the effectiveness of our method.

Algorithm 1 Robust Training in One Epoch

Input: S is the training set. f is the DNN model. $Loss$ is the loss function for training the model f .**Parameters:** \mathcal{E} is the array of the estimated sample margins. $\mathcal{E}(i)$ is the margin of the sample indexed by the unique ID i . Every $\mathcal{E}(i)$ is initialized to be Δ_ε . Δ_ε is the expansion step size (positive scalar). ξ is threshold and it is determined by using the loss values on clean data (see Section 2.2).**Output:** Updated model f after this training epoch.**Process:**

```

1: for each training sample  $(x, y)$  with ID  $i$  in  $S$  do
2:   Run the model  $f$  on clean sample:  $\hat{y} = f(x)$ 
3:   Generate a noisy sample using the PGD algorithm:  $\tilde{x} = PGD(x, y, \mathcal{E}(i))$ 
4:   Run the model  $f$  on noisy sample:  $\tilde{y} = f(\tilde{x})$ 
5:    $L_0 = Loss(\hat{y}, y)$ 
6:    $L_1 = Loss(\tilde{y}, y)$ 
7:    $L = (L_0 + L_1)/2$ 
8:   Back-propagate from  $L$  and update the model  $f$ 
9:   if  $L_1 < \xi$  then
10:     $\mathcal{E}(i) = \mathcal{E}(i) + \Delta_\varepsilon$  (Enlarge the margin)
11:   else
12:     $\mathcal{E}(i) = (\|x - \tilde{x}\|_p + \mathcal{E}(i))/2$  (Refine the margin)
13:   end if
14: end for

```

Note: The algorithm runs in mini-batches. $\|\cdot\|_p$ denotes vector L_p norm.

2 Methodology

2.1 Adaptive Margin Adversarial Training (AMAT)

In our AMAT method, the concept of “margin” is borrowed from support-vector machine [5], which means the distance between a data sample and the decision boundary of a classifier. To improve classifier robustness, during training, the generated noisy/adversarial sample should not cross the true decision boundary. Since the clean samples have different distances to the true decision boundary, the noisy samples should contain different levels of noises. In this study, although the three tasks are not simple classification, the margin concept can be generalized: the “margin” of a sample is defined as the maximum level of noise that can be added to the sample (the input) without harming the DNN performance on clean data. The basic idea of AMAT is to let each training sample have its own “margin”, instead of using a fixed noise level as SAT.

The AMAT training process is shown in Algorithm 1, which includes two sub-processes: (1) compute the loss and update the DNN model (Line 2 to 8); and (2) update the sample margins (Line 9 to 12). x is the input (clean) image, y is the DNN output (e.g., segmentation map), and i is the unique ID for the clean sample (x, y) . Given the sample i and its estimated margin $\mathcal{E}(i)$, PGD [17] is used to generate a noisy sample (Line 3). The model f runs on the clean and noisy samples to generate the outputs. Then, the loss L_0 on clean data and the loss L_1 on noisy data are calculated and combined. Finally, back-propagation runs to update the model. It is important not to add too much noise, because large noise may harm the DNN performance on clean data. To this end, we

add the condition $L_1 < \xi$ to control the noise. Generally, the loss L_1 on the noisy sample will increase if the noise level increases. In order to preserve DNN performance on clean data, the loss L_1 should not be significantly larger than the average loss value on clean data.

2.2 Value of ξ

The threshold ξ is used to determine if the noise is too large for training. Assuming that on the clean training set $S = \{(x_i, y_i) | i = 1, 2, \dots\}$, the DNN model f has been well trained; and $Loss$ is the loss function for training f on S . Then, we can obtain the loss values of all training samples, denoted by $V = \{Loss(f(x), y) | (x, y) \in S\}$. In our experiments, we observe that the distribution of the loss values approximately follows Normal distribution. The mean loss value $mean(V)$ and the standard deviation of the loss values $std(V)$ can be obtained. Then, the threshold ξ can be $mean(V)$ or $mean(V) + 2 \cdot std(V)$, and the choice is dependent on the dataset.

2.3 Loss function with multiple items

For some DNN models, the training loss function contains multiple loss terms. For instance, YOLO v5 [12] (used in Section 3.3) has three loss terms. If the loss function contains K loss terms, a small modification is made to Algorithm 1: (1) The threshold ξ becomes a vector of K scalars, and each scalar is calculated by using each of the K distributions of the loss terms on clean data; (2) Line 9 is modified to “**if** ($L_1[1] < \xi[1]$)&($L_1[2] < \xi[2]$)&...&($L_1[K] < \xi[K]$) **then**”. In short, all of the loss terms are considered separately. $mean$ and std (see Section 2.2) are computed for each loss term. When all of the loss terms on noisy data are smaller than their corresponding thresholds, the noise is acceptable for training.

3 Experiment Configuration

Three state-of-the-art DNN models and five publicly available medical image datasets are used for method evaluation. In the experiments, the model trained only on clean data is named “STD”; the model trained by the SAT method with the noise level of ε is named “SAT ε ”; the model trained by our AMAT method is called “AMAT”. All of the experiments are conducted on a server with Nvidia Tesla V100 GPU and Intel(R) Xeon(R) E5-2698 v4 CPU processor (2.20GHz). PGD-based adversarial attack is widely used for method evaluation [27, 26]. The noises for evaluation are generated by PGD with 100 iterations (which is very strong), and the noises for training are generated by PGD with 20 iterations (weaker than 100-PGD). Noise levels for evaluation are measured by L2 norm.

3.1 Evaluation on segmentation

In this experiment, we apply SAT and AMAT to a self-configuring DNN, nnUnet [11]. The nnUnet can automatically configure itself, including preprocessing,

network architecture, training, and post-processing for the dataset. The inputs of nnUnet are 2D slices of 3D images. Some of the image slices have poor quality, and the nnUnet does not filter them out, which leads to a big $std(V)$ (see Section 2.2) in the training set. As a result, in this experiment, for AMAT, ξ is set to $mean(V)$ (see Section 2.2). The ‘‘Average Dice Index (ADI)’’ is used as the metric, whose formula is:

$$ADI = \frac{1}{n} \times \sum_{i=1}^n \frac{2 \times TP_i}{2 \times TP_i + FP_i + FN_i} \quad (2)$$

Here, n is the number of samples in the test set. For the sample i , TP_i is the number of pixels in true-positive area, FP_i is the number of pixels in false-positive area, and FN_i is the number of pixels in false-negative area. The metric used in the evaluation of the nnUnet [11] is renamed ‘‘Total voxel Dice Index (TVDI)’’ in this paper, and it does not equally weight the samples. TVDI is always higher than ADI. We note that TVDI results are in the Appendix, and some are in Table 1. We use this TVDI metric to show that the clean TVDI values of our results are similar to the results reported in [11].

Three public datasets are used in this experiment. The Heart MRI dataset [24] has 20 labeled 3D images: 16 for training, 1 for validation and 3 for testing. The median shape of each 3D image is $115 \times 320 \times 320$, of which 115 is the number of slices. In this experiment, only 2D segmentation is considered, so the input of the model is one slice. The batch size (40), input image size (320×256) are self-configured by nnUnet for this data set. The model is trained for 50 epochs, where each epoch contains 50 iterations. Other training settings are the same as [11]. For SAT, we tried three different noise levels (5, 15, 25). For AMAT, the step size Δ_ϵ is 5. The Hippocampus MRI dataset [24] has 260 labeled 3D images: 208 for training, 17 for validation and 35 for testing. The median shape of each 3D image is $36 \times 50 \times 35$, where 36 is the number of slices. The batch size (366), the input image size (56×40) and network structure are self-configured by nnUnet for this data set. The model is trained for 100 epochs, where each epoch has 50 iterations. Other training settings are the same as those in [11]. For SAT, we tried four different noise levels (1, 5, 10, 15). For AMAT, the step size Δ_ϵ is 2.5. The Prostate MRI dataset [24] has 32 labeled 3D images: 25 for training, 2 for validation and 5 for testing. The median shape of each 3D image is $20 \times 320 \times 319$, where 20 is the number of slices. The batch size (32), patch size (320×320) and network structure are self-configured by nnUnet for this dataset. The model is trained for 50 epochs, where each epoch has 50 iterations. Other training settings are the same as those in [11]. For SAT, we tried three different noise levels (10, 20, 40). For AMAT, the step size Δ_ϵ is 10.

3.2 Evaluation on landmark detection

In this experiment, we apply AMAT and SAT to the Multi-Task U-Net [30]. This model detects the landmarks by regressing both Gaussian heatmap and offset maps of the landmarks simultaneously. The loss function for this model has three loss terms, and therefore ξ is a vector of size 3, of which each value

is set to $mean + 2 \cdot std$ of the corresponding loss term values (Section 2.2). The original loss function contains a Binary Cross-Entropy (BCE) loss term. We find that, by replacing the BCE loss with Dice loss, the robustness of the Multi-Task U-Net becomes much better (Section 4). The Multi-Task U-Net trained with the original loss is denoted as “STD(BCE)”, the one trained with the Dice loss is denoted as “STD(Dice)”. The two methods “SAT” and “AMAT” are applied to the “STD(Dice)” models. The metric for this experiment is “Mean Radial Error (MRE)” [30], which measures the Euclidean distance between true and predicted landmarks. MRE is scaled to the unit of mm. The dataset is created for cephalometric landmark detection in IEEE ISBI 2015 Challenge [28]. The dataset contains 400 cephalometric radiographs, which are officially split into 3 sets (Train, Test1, Test2): 150 for Train, 150 for Test1 and 100 for Test2. Because the performance of the models reported in [30] is poor on Test2, we only use Test1. Test1 is further split into 2 sets: 50 for validation and 100 for testing. Each radiograph has 19 manually labeled landmarks of clinical anatomical significance by two expert doctors. The average annotations by two doctors is considered the ground truth. The images are resized to 200×160 in our experiment. The model is trained for 500 epochs. The batch size is 8. Other training settings are the same as those in [30]. For SAT, we tried four different noise levels (1, 2, 3, 5). For AMAT, the step size Δ_ϵ is 1.

3.3 Evaluation on object detection

In this experiment, we apply AMAT and SAT to the YOLO v5s object detector [12]. The loss function has three loss terms, and therefore ξ is a vector of size 3, of which each value is set as $mean + 2 \cdot std$ of the corresponding loss term values (Section 2.2). Two metrics are used for evaluation: Average Intersection over Union (IOU) of all detected objects and mAP0.5:0.95. The dataset is named BCCD, which is a small-scale dataset for blood cell detection [23]. The dataset has 364 2D images, which is split into 3 sets: 294 for training, 33 for validation and 37 for testing. The blood cells on each image are from three classes: Red Blood Cell, White Blood Cell, and Platelets. Each image is resized to 320×320 in our experiment. The model is trained for 300 epochs. The batch size is 32. Other training settings are the same as [12]. For SAT, we tried four different noise levels (1, 5, 10, 15). For AMAT, the step size is Δ_ϵ is 2.5.

4 Results and Discussions

Segmentation results on the three datasets (Heart, Hippocampus, and Prostate): From Table 1, the TVDI values of three “STD” models are similar to those in [11], which indicates that the number of training epochs is enough for the models to converge. From Fig. 2 to 4, we have the following observations. (1) AMAT has the best performance: “AMAT” models have the largest average ADI; “AMAT” models have the highest ADI on almost all noise levels except that it is lower than “STD” on noise level 0 on the Prostate dataset. (2) The ADI

of “STD” models drops to almost 0 on the noise level 15 on the Heart dataset, on the noise level 10 on the Hippocampus dataset, and on the noise level 40 on the Prostate dataset. (3) None of the “ $SAT\varepsilon$ ” models has a good enough performance comparable to “AMAT”. (4) Compared among the “ $SAT\varepsilon$ ” models, the model with larger ε has better performance on higher-noise data, and the model with smaller ε has better performance on lower-noise data.

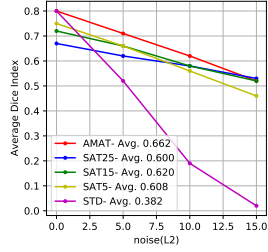


Fig. 2: ADI of nnUnet on Heart dataset

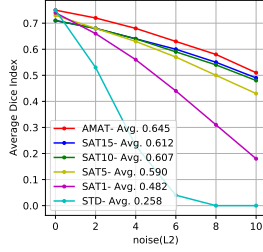


Fig. 3: ADI of nnUnet on Hippocampus dataset

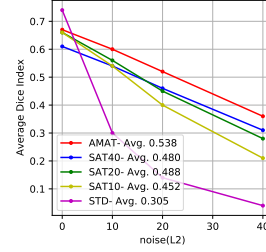


Fig. 4: ADI of nnUnet on Prostate dataset

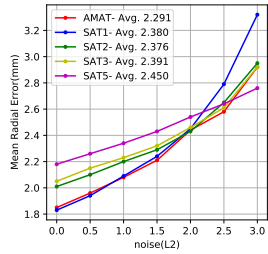


Fig. 5: MRE (mm) of Multi-Task U-Net on Cephalometric dataset

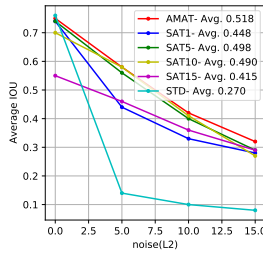


Fig. 6: Average IOU of YOLOv5s on BCCD dataset

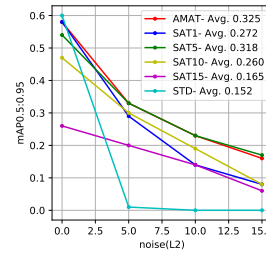


Fig. 7: mAP0.5:0.95 of YOLOv5s on BCCD dataset

Table 1: TDVI of “STD” models on three datasets

Task	TVDI
Heart	0.92
Hippocampus	0.88
Prostate	0.82

Table 2: Time cost for each training epoch (Seconds). Columns 1-3 are for segmentation; Column 4 is for landmark detection; Column 5 is for blood cell detection.

-	Heart	Hippocampus	Prostate	Landmark	BCCD
STD	31	10	20	12	6
SAT	476	114	465	50	30
AMAT	480	120	467	53	35

Table 3: MRE (mm) of Multi-Task U-Net on Cephalometric dataset (“STD” only). Because the MRE of “STD” models raise up too sharply as the noise level for evaluation increases, it is almost impossible to plot the curves of “STD” models in Fig. 5.

	noise	0	0.5	1	1.5	2	2.5	3	Avg.
STD(Dice)		1.59	3.26	7.92	18.23	28.76	36.34	36.93	19.004
STD(BCE)		1.55	4.38	14.2	27.37	37.59	42.45	45.05	24.656

Landmark detection results on the Cephalometric dataset: From Fig. 5 and Table 3, observations are as follows. (1) AMAT has the best performance:

The “AMAT” model has the smallest error. (2) “STD(Dice)” is better than “STD(BCE)”. (3) None of the “ $SAT\varepsilon$ ” models has a good enough performance comparable to “AMAT”.

Blood cell detection results on the BCCD dataset: From Fig. 6 to 7, observations are as follows. (1) AMAT has the best performance: The “AMAT” model has the largest average IOU. (2) The performance of the “STD” model drops to 0 on very small noise levels. (3) The performance of “SAT5” is close to “AMAT”. (4) Compared among the “ $SAT\varepsilon$ ” models, the model with larger ε has better performance on higher-noise data, and the model with smaller ε has better performance on lower-noise data.

Summary: (1) Our AMAT method has the best performance. (2) Table 2 shows that AMAT has almost the same training time cost as SAT. (3) The noises measured by L2 norm in the experiments are very small on each pixel, but the performance of the “STD” models drops to almost zero on small noise levels, which indicates the PGD adversarial attack with 100 iterations is a very strong and covert threat to segmentation and detection tasks. (4) In the YOLO v5s object detection experiment, “SAT5” has a performance close to “AMAT”. This suggests that “ $SAT\varepsilon$ ” with a proper ε may achieve good performance for some datasets. In general, it is difficult to find a proper ε unless a dense grid-search is used, which is extremely time-consuming (see Table 2). (5) Compared among the “ $SAT\varepsilon$ ” models, the model with larger ε has better performance on higher-noise data, and the model with smaller ε has better performance on lower-noise data, which indicates that a fixed level of noise for training is inadequate. For life-critical medical image analysis applications, the DNN models should have a good performance on both clean data and noisy data. Thus, “AMAT” with adaptive training noises is more suitable than “ $SAT\varepsilon$ ” with a fixed noise level ε .

5 Conclusion

We propose a novel adaptive adversarial training method, AMAT, to make DNNs robust against adversarial attacks/noises in medical image segmentation, landmark detection, and object detection tasks, and the key idea is to adaptively adjust the training noises for individual training samples, so that the trained DNN model will have good resistance to the adversarial noises while maintaining good accuracy on clean data. We apply our proposed method to three state-of-the-art DNNs on five publicly available medical image datasets. The experiment results show that our AMAT method outperforms the SAT method in both adversarial robustness and prediction accuracy on clean data, while having almost the same training time cost as SAT. We hope our approach may facilitate the development of robust DNNs for more medical applications in the future.

References

1. Arnab, A., Miksik, O., Torr, P.H.: On the robustness of semantic segmentation models to adversarial attacks. In: Proceedings of the IEEE Conference on Computer Vision and Pattern Recognition. pp. 888–897 (2018)
2. Brendel, W., Rauber, J., Bethge, M.: Decision-based adversarial attacks: Reliable attacks against black-box machine learning models. In: ICLR (2018)
3. Carlini, N., Wagner, D.: Towards evaluating the robustness of neural networks. In: 2017 IEEE Symposium on Security and Privacy (SP). pp. 39–57. IEEE (2017)
4. Cisse, M., Adi, Y., Neverova, N., Keshet, J.: Houdini: Fooling deep structured prediction models. arXiv preprint arXiv:1707.05373 (2017)
5. Cortes, C., Vapnik, V.: Support-vector networks. *Machine learning* **20**(3), 273–297 (1995)
6. Croce, F., Hein, M.: Reliable evaluation of adversarial robustness with an ensemble of diverse parameter-free attacks. In: International conference on machine learning. pp. 2206–2216. PMLR (2020)
7. Daza, L., Pérez, J.C., Arbeláez, P.: Towards robust general medical image segmentation. In: International Conference on Medical Image Computing and Computer-Assisted Intervention. pp. 3–13. Springer (2021)
8. Ding, G.W., Sharma, Y., Lui, K.Y.C., Huang, R.: Max-margin adversarial (mma) training: Direct input space margin maximization through adversarial training. In: ICLR (2019)
9. Goodfellow, I., Shlens, J., Szegedy, C.: Explaining and harnessing adversarial examples. In: ICLR (2015)
10. He, X., Yang, S., Li, G., Li, H., Chang, H., Yu, Y.: Non-local context encoder: Robust biomedical image segmentation against adversarial attacks. In: Proceedings of the AAAI Conference on Artificial Intelligence. vol. 33, pp. 8417–8424 (2019)
11. Isensee, F., Jaeger, P.F., Kohl, S.A., Petersen, J., Maier-Hein, K.H.: nnu-net: a self-configuring method for deep learning-based biomedical image segmentation. *Nature methods* **18**(2), 203–211 (2021)
12. Jocher, G., Chaurasia, A., et al.: ultralytics/yolov5: v6.1 - TensorRT, TensorFlow Edge TPU and OpenVINO Export and Inference (Feb 2022). <https://doi.org/10.5281/zenodo.6222936>, <https://doi.org/10.5281/zenodo.6222936>
13. Joel, M.Z., Umrao, S., Chang, E., Choi, R., Yang, D., Duncan, J., Omuro, A., Herbst, R., Krumholz, H., Aneja, S., et al.: Adversarial attack vulnerability of deep learning models for oncologic images. medRxiv pp. 2021–01 (2021)
14. Kurakin, A., Goodfellow, I., Bengio, S.: Adversarial machine learning at scale. In: ICLR (2017)
15. Liu, Q., Jiang, H., Liu, T., Liu, Z., Li, S., Wen, W., Shi, Y.: Defending deep learning-based biomedical image segmentation from adversarial attacks: a low-cost frequency refinement approach. In: International Conference on Medical Image Computing and Computer-Assisted Intervention. pp. 342–351. Springer (2020)
16. Ma, L., Liang, L.: Increasing-margin adversarial (ima) training to improve adversarial robustness of neural networks. arXiv preprint arXiv:2005.09147 (2020)
17. Madry, A., Makelov, A., Schmidt, L., Tsipras, D., Vladu, A.: Towards deep learning models resistant to adversarial attacks. In: ICLR (2018)
18. Moosavi-Dezfooli, S.M., Fawzi, A., Frossard, P.: Deepfool: a simple and accurate method to fool deep neural networks. In: Proceedings of the IEEE conference on computer vision and pattern recognition. pp. 2574–2582 (2016)

19. Mummadi, C.K., Brox, T., Metzen, J.H.: Defending against universal perturbations with shared adversarial training. In: Proceedings of the IEEE/CVF International Conference on Computer Vision. pp. 4928–4937 (2019)
20. Ozbulak, U., Van Messem, A., Neve, W.D.: Impact of adversarial examples on deep learning models for biomedical image segmentation. In: International Conference on Medical Image Computing and Computer-Assisted Intervention. pp. 300–308. Springer (2019)
21. Paschali, M., Conjeti, S., Navarro, F., Navab, N.: Generalizability vs. robustness: investigating medical imaging networks using adversarial examples. In: International Conference on Medical Image Computing and Computer-Assisted Intervention. pp. 493–501. Springer (2018)
22. Shafahi, A., Najibi, M., Ghiasi, M.A., Xu, Z., Dickerson, J., Studer, C., Davis, L.S., Taylor, G., Goldstein, T.: Adversarial training for free! In: Advances in Neural Information Processing Systems. vol. 32 (2019)
23. Shenggan: Bccd dataset (2017), <https://github.com/Shenggan/BCCDDataset>
24. Simpson, A.L., Antonelli, M., Bakas, S., Bilello, M., Farahani, K., Van Ginneken, B., Kopp-Schneider, A., Landman, B.A., Litjens, G., Menze, B., et al.: A large annotated medical image dataset for the development and evaluation of segmentation algorithms. arXiv preprint arXiv:1902.09063 (2019)
25. Szegedy, C., Zaremba, W., Sutskever, I., Bruna, J., Erhan, D., Goodfellow, I., Fergus, R.: Intriguing properties of neural networks. In: ICLR (2014)
26. Tramer, F., Carlini, N., Brendel, W., Madry, A.: On adaptive attacks to adversarial example defenses. Advances in Neural Information Processing Systems **33**, 1633–1645 (2020)
27. Uesato, J., O’donoghue, B., Kohli, P., Oord, A.: Adversarial risk and the dangers of evaluating against weak attacks. In: International Conference on Machine Learning. pp. 5025–5034. PMLR (2018)
28. Wang, C.W., Huang, C.T., Lee, J.H., Li, C.H., Chang, S.W., Siao, M.J., Lai, T.M., Ibragimov, B., Vrtovec, T., Ronneberger, O., et al.: A benchmark for comparison of dental radiography analysis algorithms. Medical image analysis **31**, 63–76 (2016)
29. Xie, C., Wang, J., Zhang, Z., Zhou, Y., Xie, L., Yuille, A.: Adversarial examples for semantic segmentation and object detection. In: Proceedings of the IEEE international conference on computer vision. pp. 1369–1378 (2017)
30. Yao, Q., He, Z., Han, H., Zhou, S.K.: Miss the point: targeted adversarial attack on multiple landmark detection. In: International Conference on Medical Image Computing and Computer-Assisted Intervention. pp. 692–702. Springer (2020)
31. Zhang, H., Wang, J.: Towards adversarially robust object detection. In: Proceedings of the IEEE/CVF International Conference on Computer Vision. pp. 421–430 (2019)
32. Zhu, C., Li, X., Li, J., Dai, S.: Improving robustness of facial landmark detection by defending against adversarial attacks. In: Proceedings of the IEEE/CVF International Conference on Computer Vision. pp. 11751–11760 (2021)